

Article

Induction Machine On-Line Parameter Identification for Resource-Constrained Microcontrollers Based on Steady-State Voltage Model

Tomas Kostal *  and Pavel Koblre 

Department of Electric Drives and Traction, Czech Technical University in Prague, 166 27 Prague, Czech Republic; kobrlpav@fel.cvut.cz

* Correspondence: kostatom@fel.cvut.cz

Abstract: This paper presents a new, computationally modest on-line identification method for the simultaneous estimation of the rotor resistance and magnetizing inductance of an induction machine suitable for electric drives that use an indirect field-oriented control strategy (IFOC), and their control hardware is equipped with a resource-constrained microcontroller. Such drives can be found both in the manufacturing industry and railway traction vehicles in the thousands, having either older control hardware that cannot cope with computationally excessive identification methods or being in cost-sensitive applications, thus being equipped with a low-cost microcontroller. IFOC is a very common control strategy for such drives due to its good dynamic properties and comparatively simple implementation. However, it is sensitive to inaccuracies of rotor resistance and magnetizing inductance. These two parameters change during the operation of the drive, being influenced by the temperature, frequency, and saturation of the magnetic circuit. Improper values of parameters in the controller can degrade the performance of IFOC, resulting in slower acceleration or unnecessary oversaturation of the machine. Respecting these changes can therefore bring significant benefits such as the good dynamic properties of the drive, which can shorten operations in the manufacturing industry or travel times of vehicles. A number of on-line identification methods for monitoring the parameter changes have been published so far, but the majority of them are demanding on microcontroller time or its memory. The proposed method, on the contrary, is comparatively simple and thus easy for implementation with low requirements to the microcontroller. Therefore, it is suitable for both upgrades of existing drives or new low-cost applications. Derivation of the method from the mathematical model and the final algorithm for the microcontroller are presented. The performance of the proposed method is validated with experimental results obtained with a 3.5 kW induction machine drive with an industrial microcontroller during a warming test and under various loads and frequencies.

Keywords: induction motor drives; rotor resistance; magnetizing inductance; on-line parameter identification; resource-constrained microcontrollers



Citation: Kostal, T.; Koblre, P. Induction Machine On-Line Parameter Identification for Resource-Constrained Microcontrollers Based on Steady-State Voltage Model. *Electronics* **2021**, *10*, 1981. <https://doi.org/10.3390/electronics10161981>

Academic Editor: Nicu Bizon

Received: 25 June 2021

Accepted: 10 August 2021

Published: 17 August 2021

Publisher's Note: MDPI stays neutral with regard to jurisdictional claims in published maps and institutional affiliations.



Copyright: © 2021 by the authors. Licensee MDPI, Basel, Switzerland. This article is an open access article distributed under the terms and conditions of the Creative Commons Attribution (CC BY) license (<https://creativecommons.org/licenses/by/4.0/>).

1. Introduction

Induction machines have many favorable properties such as robustness, reliability, and low maintenance cost, which have caused them to become one of the most widespread types of electromechanical converters in industrial and railway applications. Probably the most significant difficulty of induction machines is the complexity of their control when they are used in a variable speed drive. Among various modern methods of control of induction machines, Field-Oriented Control (FOC), Model Predictive Control (MPC), and Direct Torque Control (DTC) are the most frequently used ones [1–9]. All these methods of control have a common feature in that they rely on some form of mathematical model of the induction machine.

The model of the induction machine is characterized by a set of parameters. This set of parameters can vary based on the complexity of the mathematical model used, the purpose of the model, or the phenomena of the machine that are being studied. One of the most common sets of parameters representing an induction machine model consists of the following five parameters: stator resistance R_s , rotor resistance R_r , stator leakage inductance $L_{\sigma s}$, rotor leakage inductance $L_{\sigma r}$, and magnetizing inductance L_m [1,5,10–12].

The precision of knowledge of the machine parameters can have a great influence on the performance of the control algorithm. Unfortunately, out of the parameters mentioned in the previous paragraph, only R_s is directly measurable in the case of induction machines with squirrel cage rotor. When the induction machine has a wound rotor, then R_r is also directly measurable via slip rings; however, this type of machine comprises only a minority of installations compared to the squirrel cage type. Therefore, a number of indirect methods have been developed to identify the machine parameters. When laboratory equipment is available, standard tests (no-load, locked rotor test, and DC measurement) are used [5,11,13–15]. So-called off-line or self-commissioning methods serve to acquire parameter values before the start of the operation [5,11,14–18] of the drive in the place of its installation. These methods thus acquire values of parameters corresponding to the state of the machine at the moment of their execution. These values can have great accuracy, but they cannot reflect the changes of some of the parameters during the operation of the drive that are being influenced by temperature, frequency, or saturation. Firstly, temperature directly affects the resistance of metal conductors; thus, the increasing temperature of the machine leads to an increase in stator and rotor resistance [5,11,19]. The temperature dependence of inductances is not observable under normal operational conditions of the machine [11]. Secondly, frequency can affect the value of resistances due to the skin effect. Stator winding of the machine is, however, usually made out of multiple parallel conductors, which prevent the skin effect caused by supply frequency. However, the skin effect can be observed in rotor cage conductors (of squirrel cage rotors) as they have a larger cross section. As the slip of the machine rises, the slip frequency rises as well, increasing the value of effective rotor resistance [5,11,19]. Thirdly, saturation influences magnetizing inductance, which decreases with rising magnetic flux (or stator current magnetizing component) [5,11]. Fluxes of leakage inductances represent mainly the magnetic field that closes through the air, which cannot be saturated, so their values are considered stable [11,20].

Different control algorithms stress the importance of different parameters [5,15,18]. For the rotor-flux-oriented indirect field-oriented control (IFOC), which is among the most widespread control strategies, rotor resistance and magnetizing inductance can be considered the most crucial ones [5,12,21,22]. The main idea behind IFOC is to control the induction machine similarly to a DC machine with a separate control of the so-called torque and flux component of the induction machine stator current. This virtual decomposition is achieved with the help of these two parameters and mathematical transforms. With incorrect values of these two parameters, the stator current is decomposed into incorrect components. The controllers in the control structure try to correct these errors, but if, for example, the controller expects a lower flux component than the real one, it can lead to an unwanted oversaturation of the magnetic circuit. With an error in the torque component, it can take longer for the controller to adjust the torque to the desired value, thus reducing the acceleration of the drive [5,12]. Tracking the machine parameter changes is thus beneficial even in the case of drives with control systems with limited computational resources.

A number of different so-called on-line methods were developed for monitoring machine parameters during operation. However, a lot of them are computationally demanding or demanding on the memory and thus are not suitable for microcontrollers with limited resources.

Among the most demanding ones are Artificial Neural Networks (ANN), Genetic Algorithms (GAs), and Optimization Algorithms (OAs) [5]. ANNs are characterized by the need to have training samples or a training algorithm, which requires extra time and

resources. It can be so demanding that for its implementation a microcontroller with a real-time control accelerator may be needed [6]. GAs are demanding on the storage of historical data, while OAs, such as Particle Swarm Optimization, need a large number of calculations [23].

Different types of observers are another vast group of methods used. The Luenberger observer was used for flux estimation with an ensuing stator and rotor resistance calculation in [24] and for a stator resistance estimation in [25,26]. Sliding mode observer usage for stator resistance estimation has been proposed in [27]. An adaptive observer for stator and rotor resistance was utilized in [28]. These observer-based methods need matrix calculations in their algorithms, which can be a limiting point for their deployment in a microcontroller with resource-constrained hardware.

The Extended Kalman Filter (EKF) has also been widely studied for parameter identification [29–31], but this method is also characterized by its excessive computational demands [5].

Recursive Least Square (RLS) [10,32,33] is easy to implement and is not so computationally intensive, but it is very sensitive to noise [34], which implies the implementation of more sophisticated filters. Additionally, the tuning of the forgetting factor of RLS can be tricky [5] and can lead to error accumulation. To overcome this, a time-varying forgetting factor has been proposed [35], which, however, makes the RLS more complex.

Model Reference Adaptive System (MRAS)-based methods can be also counted among computationally undemanding techniques with a simple structure and implementation [21,22,36,37]. Usually, they are used to identify one or two parameters because it is difficult to find a stable adaptive law [5]. The adaptive law is often implemented by PI or I controllers, which can be seen as a burden from the point of view of limited-resources hardware because it needs an additional controller in the structure.

Signal injection is generally not demanding on the microcontroller, but it brings other related difficulties with its implementation. The use of a high-frequency signal is not so popular because of its demands on the speed of the switching devices of the converter [5]. DC signal injection is thus more favorable; however, it can cause unwanted additional torque pulsations. These could be avoided, for instance, by introducing second-order harmonics [38], which can lead to more complicated structures in the microcontroller. Further, it should be used only in specified time spans to avoid unnecessary additional power losses caused by the DC test signal [39].

Among the methods that do not require excessive microcontroller resources are those based on voltage model calculation. In [40], the authors used voltage-model-derived differential equations to calculate rotor resistance and magnetizing inductance. If at least a part of the working cycle of the drive can be considered steady-state, a steady-state model of the machine can be used, which enables the usage of algebraic equations which are far less complex to solve [22].

Another area of computationally modest approaches is based on compensations of machine resistances based on temperature measurements. In [19], the authors used a temperature sensor mounted to the stator winding of the machine. Based on the temperature change, they calculated the values of both stator and rotor resistances assuming that the temperature of the whole machine is the same. In [41], the authors also equipped the rotor of a machine with a wireless temperature sensor besides the wired one attached to the stator winding. However, a temperature sensor is usually not standard equipment of a machine and has to be mounted additionally, which can be seen as a burden, especially in the case of a rotor temperature sensor.

In general, additional sensors are not favored due to cost and reliability reasons, which has led to a great advent of so-called sensor-less drives in recent years. However, a number of drives are still equipped with a speed sensor, which can be used to help with parameter identification. Such examples can be found in the manufacturing industry [42–44] or railway traction vehicles (locomotives, EMUs) [45], where induction machines are still the dominant type of electromechanical converter. Other sensors used in industrial or

traction electric drives are current sensors on machine terminals and voltage sensors in the DC-links of power converters [44,46]. A method suitable for parameter identification of the drive with a microcontroller with limited resources should only use the quantities that are already measurable within the standard drive configuration.

The combination of a steady-state voltage model and information from a mechanical speed sensor was used in [12]. Stator voltages and currents, stator frequency, and mechanical frequency measured with a speed sensor were used to calculate rotor resistance to obtain the temperature change of the rotor of the induction machine in a battery electric vehicle drive. In [22], the same combination was used for the estimation of rotor magnetic flux and its angle.

This paper proposes the new method of the simultaneous on-line identification of rotor resistance and magnetizing inductance suitable for IFOC. This method has significantly lower computational demands than those mentioned in the introduction as it does not need excessive calculations, nor does it need to store large data in memory. It does not need any additional PI or I controllers in its structure and does not need to solve any differential equations. It is focused on drives with induction machines that are equipped with a mechanical speed sensor, a microcontroller with limited resources and where a part of their working cycle is in a steady-state mode. These could be existing drives with an older microcontroller system whose hardware cannot cope with computational or memory-intensive algorithms or new drives that need a speed sensor due to technical standards, or for high precision speed or position measurement, but otherwise are equipped with low-cost microcontrollers.

2. Drive with Field-Oriented Control

A block scheme of a variable-speed industrial drive with an induction machine is shown in Figure 1. As the voltage measurement of the switched voltage at the output of the inverter is complicated due to its rectangular nature with steep rising and falling edges, voltage is usually reconstructed from the switching pattern and the measured DC-link voltage that normally has far slower changes [17]. The nonlinearity of the inverter is also taken into account in most cases [12,46]. With the help of this procedure, stator voltage and frequency (or angular speed of the stator magnetic field) are obtained. Current sensors for measuring the machine stator current are placed on the inverter output, normally on two phases, while the third current is calculated from the other two [44]. A speed sensor is mounted on the shaft of the machine or on the gearbox, giving the information about the mechanical speed of the machine [8,45].

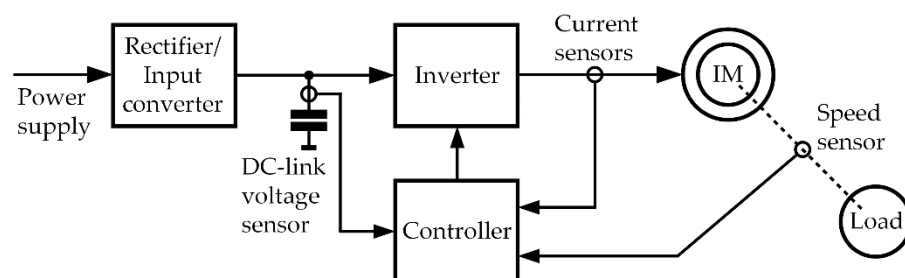


Figure 1. Structure of a common drive with induction machine.

The controller of the drive is thus enabled to acquire stator current components I_{sd} and I_{sq} , stator voltage components V_{sd} and V_{sq} , stator angular frequency ω_s and rotor angular frequency ω_m . The proposed identification method requires no other quantities or sensors than these.

3. Mathematical Model of the Machine

An induction machine mathematical model is usually represented by an equivalent circuit scheme. For the parameters mentioned in the introduction (stator resistance R_s , rotor resistance R_r , stator leakage inductance $L_{\sigma s}$, rotor leakage inductance $L_{\sigma r}$, and magnetizing inductance L_m), the so-called T-equivalent circuit is used (Figure 2).

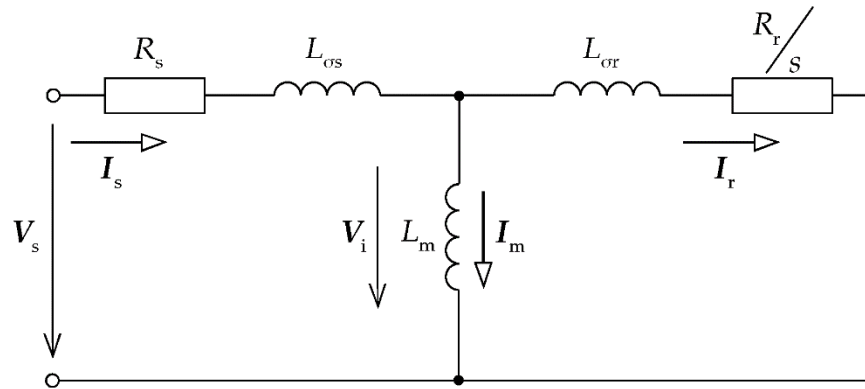


Figure 2. T-equivalent circuit of an induction machine.

This circuit is derived based on the following vector equations that describe the induction machine in steady-state with harmonic supply:

$$V_s = R_s \cdot I_s + j \cdot \omega_s \cdot L_{\sigma s} \cdot I_s + V_i, \quad (1)$$

$$V_i = j \cdot \omega_s \cdot L_m \cdot I_m, \quad (2)$$

$$V_i = \frac{R_r}{s} \cdot I_r + j \cdot \omega_s \cdot L_{\sigma r} \cdot I_r, \quad (3)$$

$$I_m = I_s - I_r, \quad (4)$$

with the meaning of particular designations shown in Nomenclature.

These vector equations can also be expressed in the form of their components in a dq reference frame, which is a common form of representation of vectors in microcontrollers. Capital letters are used for respective vector components to denote that they are steady-state values. The component notation of Equations (1)–(4) is:

$$\begin{aligned} V_{sd} &= R_s \cdot I_{sd} - \omega_s \cdot L_{\sigma s} \cdot I_{sq} + V_{id} \\ V_{sq} &= R_s \cdot I_{sq} + \omega_s \cdot L_{\sigma s} \cdot I_{sd} + V_{iq} \end{aligned} \quad (5)$$

$$\begin{aligned} V_{id} &= -\omega_s \cdot L_m \cdot I_{mq} \\ V_{iq} &= \omega_s \cdot L_m \cdot I_{md} \end{aligned} \quad (6)$$

$$\begin{aligned} V_{id} &= \frac{R_r}{s} \cdot I_{rd} - \omega_s \cdot L_{\sigma r} \cdot I_{rq} \\ V_{iq} &= \frac{R_r}{s} \cdot I_{rq} + \omega_s \cdot L_{\sigma r} \cdot I_{rd} \end{aligned} \quad (7)$$

and

$$\begin{aligned} I_{md} &= I_{sd} - I_{rd} \\ I_{mq} &= I_{sq} - I_{rq} \end{aligned} \quad (8)$$

3.1. Solution of the Mathematical Model for Calculating Rotor Resistance R_r and Magnetizing Inductance L_m

Values of I_{sd} , I_{sq} , V_{sd} , V_{sq} , ω_s , and ω_r are supposed to be known in the microcontroller, as described in Section 2. Further, the values of parameters $L_{\sigma s}$, $L_{\sigma r}$, and R_s are also assumed to be known, either provided by the manufacturer or by standard (laboratory) tests [13] or some off-line method. Aspects of using these three parameters are further discussed in

Section 5. Assuming the steady-state of the machine, all those quantities are assumed to be constant during the calculation.

Back EMF components V_{id} and V_{iq} can be calculated from Equation (5) as all the other quantities are known:

$$\begin{aligned} V_{id} &= V_{sd} + \omega_s \cdot L_{\sigma s} \cdot I_{sq} - R_s \cdot I_{sd} \\ V_{iq} &= V_{sq} - \omega_s \cdot L_{\sigma s} \cdot I_{sd} - R_s \cdot I_{sq} \end{aligned} \quad (9)$$

One of the vectors, e.g., the stator voltage, can be aligned with an axis of the dq reference frame, resulting in the particular component of such a vector being equal to zero. This zero component could possibly be omitted from the notation of the equations, but for generality it is assumed in this paper that the vectors can have any position.

For the clarity and simplification of the notation of the calculation, equivalent rotor resistance R_{req} is defined as:

$$R_{req} = \frac{R_r}{s} = R_r \cdot \frac{\omega_s}{\omega_s - \omega_m} \quad (10)$$

Rotor current components I_{rd} and I_{rq} can be calculated by merging and rearranging Equation (7):

$$\begin{aligned} I_{rd} &= \frac{R_{req} \cdot V_{id} + \omega_s \cdot L_{\sigma r} \cdot V_{iq}}{R_{req}^2 + \omega_s^2 \cdot L_{\sigma r}^2} \\ I_{rq} &= \frac{R_{req} \cdot V_{iq} - \omega_s \cdot L_{\sigma r} \cdot V_{id}}{R_{req}^2 + \omega_s^2 \cdot L_{\sigma r}^2} \end{aligned} \quad (11)$$

From the equivalent circuit (Figure 2), it is obvious that magnetizing current components I_{md} and I_{mq} can be expressed not only as stated in Equation (8), but also as:

$$\begin{aligned} I_{md} &= \frac{V_{iq}}{\omega_s \cdot L_m} \\ I_{mq} &= -\frac{V_{id}}{\omega_s \cdot L_m} \end{aligned} \quad (12)$$

Substituting I_{md} and I_{mq} from Equation (12) to Equation (8) and I_{rd} and I_{rq} from Equation (11) to Equation (8), Equation (8) can be rewritten as:

$$\begin{aligned} \frac{V_{iq}}{\omega_s \cdot L_m} &= I_{sd} - \frac{R_{req} \cdot V_{id} - \omega_s \cdot L_{\sigma r} \cdot V_{iq}}{R_{req}^2 + \omega_s^2 \cdot L_{\sigma r}^2} \\ -\frac{V_{id}}{\omega_s \cdot L_m} &= I_{sq} - \frac{R_{req} \cdot V_{iq} + \omega_s \cdot L_{\sigma r} \cdot V_{id}}{R_{req}^2 + \omega_s^2 \cdot L_{\sigma r}^2} \end{aligned} \quad (13)$$

Converting I_{sd} and I_{sq} to a common denominator with the rest of the right side of Equation (13) forms:

$$\begin{aligned} \frac{V_{iq}}{\omega_s \cdot L_m} &= \frac{R_{req}^2 \cdot I_{sd} + \omega_s^2 \cdot L_{\sigma r}^2 \cdot I_{sd} - R_{req} \cdot V_{id} - \omega_s \cdot L_{\sigma r} \cdot V_{iq}}{R_{req}^2 + \omega_s^2 \cdot L_{\sigma r}^2} \\ -\frac{V_{id}}{\omega_s \cdot L_m} &= \frac{R_{req}^2 \cdot I_{sq} + \omega_s^2 \cdot L_{\sigma r}^2 \cdot I_{sq} - R_{req} \cdot V_{iq} + \omega_s \cdot L_{\sigma r} \cdot V_{id}}{R_{req}^2 + \omega_s^2 \cdot L_{\sigma r}^2} \end{aligned} \quad (14)$$

Now, the first equation in Equation (14) is multiplied with V_{id} and the second equation in Equation (14) is multiplied with V_{iq} , and the values are then added together to eliminate the left sides and obtain Equation (15):

$$\begin{aligned} 0 &= \frac{R_{req}^2 \cdot I_{sd} \cdot V_{id} + \omega_s^2 \cdot L_{\sigma r}^2 \cdot I_{sd} \cdot V_{id} - R_{req} \cdot V_{id}^2 - \omega_s \cdot L_{\sigma r} \cdot V_{iq} \cdot V_{id}}{R_{req}^2 + \omega_s^2 \cdot L_{\sigma r}^2} + \\ &+ \frac{R_{req}^2 \cdot I_{sq} \cdot V_{iq} + \omega_s^2 \cdot L_{\sigma r}^2 \cdot I_{sq} \cdot V_{iq} - R_{req} \cdot V_{iq}^2 + \omega_s \cdot L_{\sigma r} \cdot V_{id} \cdot V_{iq}}{R_{req}^2 + \omega_s^2 \cdot L_{\sigma r}^2} \end{aligned} \quad (15)$$

Rearranging the matching constituents of Equation (15) forms:

$$0 = \frac{R_{\text{req}}^2 \cdot (I_{\text{sd}} \cdot V_{\text{id}} + I_{\text{sq}} \cdot V_{\text{iq}}) + \omega_s^2 \cdot L_{\text{or}}^2 \cdot (I_{\text{sd}} \cdot V_{\text{id}} + I_{\text{sq}} \cdot V_{\text{iq}}) - R_{\text{req}} \cdot (V_{\text{id}}^2 + V_{\text{iq}}^2)}{R_{\text{req}}^2 + \omega_s^2 \cdot L_{\text{or}}^2}. \quad (16)$$

As the left side of Equation (16) is equal to zero, the denominator can be removed. The expression in the nominator of Equation (16) can be rearranged as:

$$R_{\text{req}}^2 - R_{\text{req}} \cdot \frac{V_{\text{id}}^2 + V_{\text{iq}}^2}{I_{\text{sd}} \cdot V_{\text{id}} + I_{\text{sq}} \cdot V_{\text{iq}}} + \omega_s^2 \cdot L_{\text{or}}^2 = 0, \quad (17)$$

which is a reduced quadratic equation of the type $x^2 + px + q = 0$ that can be solved by the common formula for finding its roots. For clarity, the denominator of p is defined as an inner power of the machine P_i and the nominator of p as a squared magnitude of a back EMF vector $|V_i|^2$:

$$\begin{aligned} P_i &= I_{\text{sd}} \cdot V_{\text{id}} + I_{\text{sq}} \cdot V_{\text{iq}} \\ |V_i|^2 &= V_{\text{id}}^2 + V_{\text{iq}}^2 \end{aligned} \quad (18)$$

For the motoric mode of the machine, the inner power P_i is positive and therefore the positive sign of the square root in the quadratic formula is used:

$$R_{\text{req}} = \frac{1}{2} \left(\frac{|V_i|^2}{P_i} + \sqrt{\left(\frac{|V_i|^2}{P_i} \right)^2 + 4 \cdot \omega_s^2 \cdot L_{\text{or}}^2} \right). \quad (19)$$

If the machine acts as a generator (regenerative braking), then the inner power is negative and therefore the negative sign is used, which is shown in Equation (20). The resulting value of R_{req} will then be negative. Despite this, the resulting value of R_r will be positive, as the value of slip s is also negative in the regenerative brake mode of the machine.

$$R_{\text{req}} = \frac{1}{2} \left(\frac{|V_i|^2}{P_i} - \sqrt{\left(\frac{|V_i|^2}{P_i} \right)^2 + 4 \cdot \omega_s^2 \cdot L_{\text{or}}^2} \right). \quad (20)$$

The final value of R_r is then easily calculated from R_{req} by multiplying it with slip s . With a known value of R_{req} (or R_r), magnetizing inductance L_m can be calculated from the second or preferably the first equation of Equation (12) as it does not contain a negative sign. The calculation is performed only with half of the components of the vectors V_i and I_m , which can have different signs based on actual vector positions. To prevent the negative resulting value of L_m , the absolute value of the right side is added, forming the final equation for calculating L_m as:

$$L_m = \left| \frac{V_{\text{iq}}}{\omega_s \cdot I_{\text{md}}} \right|. \quad (21)$$

As deriving the calculation is based on a vector description that can be in the scale of both maximum values (amplitudes) or RMS values, the calculation gives the same results both for maximum or RMS input values.

3.2. Algorithm for Calculation in Microcontroller

To summarize the previous deduction, a list of equations (Algorithm 1) that need to be performed by the microcontroller is presented in this chapter. Maximum or RMS values of input quantities can be used, considering particular implementation. First, back EMF components are calculated from stator current and voltage (Equations (a) and (b)). Then, the inner power (Equation (c)) and squared magnitude of the back EMF vector (Equation (d)) values are needed for the coefficient p (Equation (e)) of the reduced quadratic

equation. The q coefficient is calculated in Equation (f) and the discriminant in Equation (g). Following the equivalent rotor resistance R_{req} calculation (Equation (h)), its value is used to calculate the rotor current component (Equation (i)). In the denominator of Equation (i), the value of the q component is used once again as this part has the same value (see Equation (11)). The rotor current component is needed for the magnetizing current component calculation (Equation (j)). With the value of the magnetizing current component, L_m can finally be calculated (Equation (k)). Rotor resistance R_r could be calculated already after Equation (h), but is left till the end of the calculation in order to have the resulting values of parameters in the last two equations. So, in Equation (l), R_{req} is multiplied by the value of the actual slip s (see Equation (10)) to obtain the R_r .

Algorithm 1. Proposed method for simultaneous estimation of R_r and L_m .

$$\begin{aligned}
 V_{id} &= V_{sd} + \omega_s \cdot L_{\sigma s} \cdot I_{sq} - R_s \cdot I_{sd} & (a) \\
 V_{iq} &= V_{sq} - \omega_s \cdot L_{\sigma s} \cdot I_{sd} - R_s \cdot I_{sq} & (b) \\
 P_i &= V_{id} \cdot I_{sd} + V_{iq} \cdot I_{sq} & (c) \\
 |V_i|^2 &= V_{id}^2 + V_{iq}^2 & (d) \\
 p &= \frac{|V_i|^2}{P_i} & (e) \\
 q &= \omega_s^2 \cdot L_{\sigma r}^2 & (f) \\
 D &= p^2 - 4 \cdot q & (g) \\
 R_{req} &= \frac{p + \sqrt{D}}{2} & (h) \\
 I_{rd} &= \frac{R_{req} \cdot V_{id} + \omega_s \cdot L_{\sigma r} \cdot V_{iq}}{R_{req}^2 + q} & (i) \\
 I_{md} &= I_{sd} - I_{rd} & (j) \\
 L_m &= \left| \frac{V_{iq}}{\omega_s \cdot I_{md}} \right| & (k) \\
 R_r &= R_{req} \cdot \frac{\omega_s - \omega_m}{\omega_s} & (l)
 \end{aligned}$$

4. Experimental Results

The proposed method was verified experimentally on a laboratory drive with a squirrel cage induction machine with a rated power of 3.5 kW coupled to a 9.4 kW DC machine. The structure of this test bench is depicted in Figure 3.

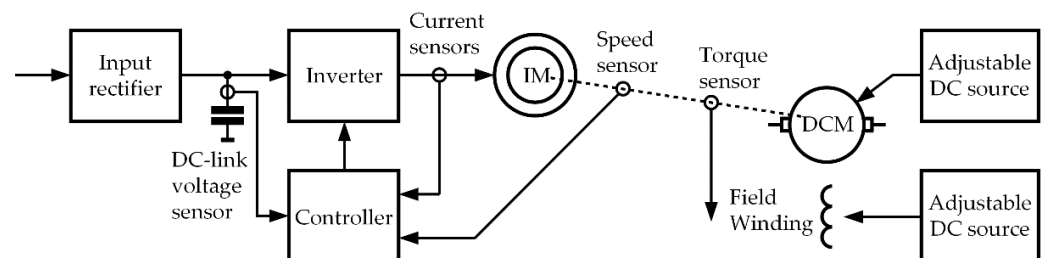


Figure 3. Test bench block scheme.

Rated values are in Table 1 and parameters obtained by standard tests (laboratory measurements) according to [13] are in Table 2.

Table 1. Tested machine rated parameters (type 1AY112L-6, producer: EM Brno Ltd.).

Rated Values		Construction Details	
Rated power P_n	3.5 kW	Number of poles	2p = 6
Rated supply voltage V_{sn}	380 V	Connection	Y
Rated supply frequency f_{sn}	50 Hz	Type of rotor	Squirrel cage
Rated current I_{sn}	11 A	Rotor conductor material	Copper
Rated $\cos \phi$	0.6	Class of insulation	F
Rated efficiency η	80.6%	Type of construction	IM2001
Rated speed n_n	965 min ⁻¹	Type of cooling	IC416
Rated torque T_n	30 N·m	$L_{\sigma s} : L_{\sigma r}$ ratio	1:1
Rated moment of inertia J	0.07 kg·m ²		

Table 2. Values of parameters of tested machine used for calculations obtained by standard tests specified in [13].

Parameter	Value
Stator resistance R_s	1.11 Ω
Stator leakage inductance $L_{\sigma s}$	8.25 mH
Rotor leakage inductance $L_{\sigma r}$	8.25 mH

Other components of the test bench (see Figure 4) were a two-level three-phase voltage type DC/AC IGBT inverter, voltage transducer LEM LV25-P for DC-link voltage measurement and current transducers LEM LF205-S for stator current measurement. Stator voltage and its angular frequency were obtained as described in Section 2. Rotor mechanical speed was measured with a LARM IRC 300/1024 optical incremental encoder with 1024 impulses per revolution.

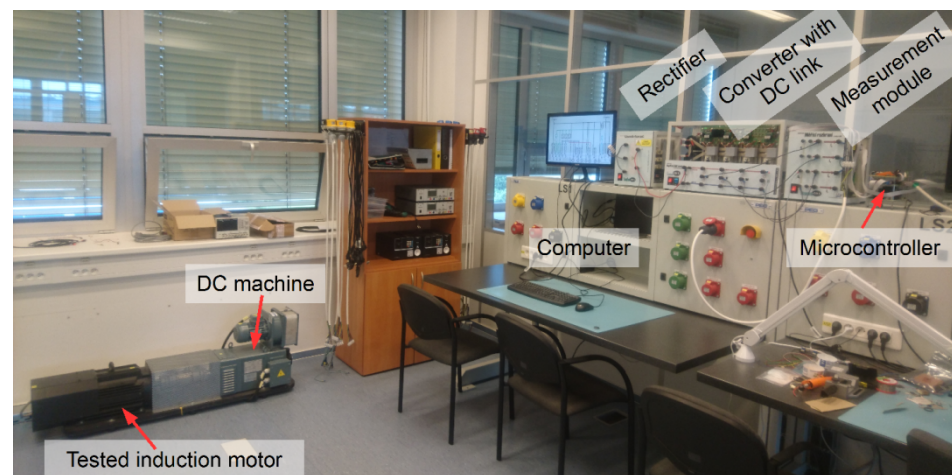


Figure 4. Picture of the test bench.

The heart of the control system was a TI TM4C123G-H6PM microcontroller with 12-bit successive approximation AD converters. For torque measurements, a torque-measuring shaft KTR DATAFLEX 22/100 was used.

As stated at the end of Section 3.1, maximum (amplitudes) or RMS input values can be chosen for input. The following experiments use maximum values in all cases. The voltage vector is aligned with the q axis, so the d component (V_{sd}) is zero in all presented cases.

4.1. Warming Test

To observe how the method can track the two parameters in the course of time, a 60 min long warming test with a constant load (6 N·m) was performed. The change in rotor resistance R_r and frame warming is depicted in Figure 5.

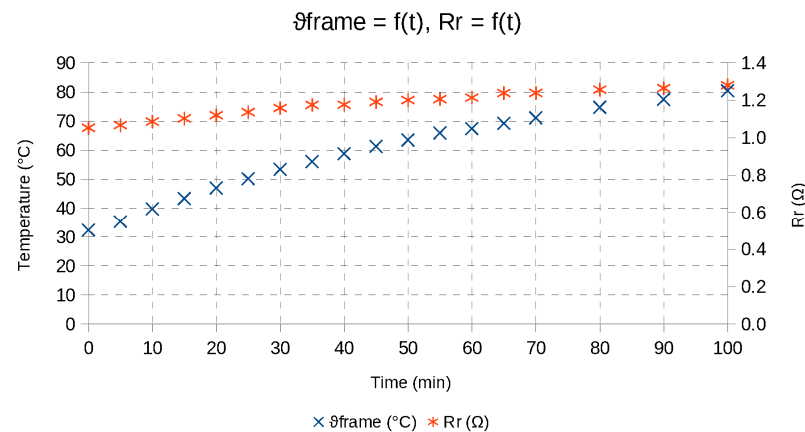


Figure 5. R_r and machine frame temperature θ_{frame} change during warming test.

Data for each point were averaged from 12 sets of samples of input quantities, and the time span between these samples was 10 s. The temperature of the machine frame was measured with a PT100 sensor. The initial temperature was 32 °C and the final temperature was 80 °C, resulting in a warming of 48 °C. R_r rose from 1.05 Ω to 1.28 Ω, which is an increase of 22%. Considering the well-known equation for the temperature dependence of metals (Equation (22)), and assuming the linear behavior of this dependence, this change in resistance estimated by the proposed method is in good accordance with it.

$$R_{\theta 2} = R_{20} \cdot (1 + \alpha_{20} \cdot \Delta\theta) = R_{20} \cdot (1 + 0.0038 \cdot 48) = 1.18 \cdot R_{20}, \quad (22)$$

where $\Delta\theta = 48$ °C (warming during our test) and $\alpha_{20} = 0.0038$ K⁻¹ is the temperature coefficient for copper (material of the cage of the tested machine). The result of Equation (22) means a rise of 18% from the initial value R_{20} compared to 22% obtained by the proposed method. It is correct that the value obtained by this method is higher than that obtained by the temperature change of the stator. The temperature of the rotor is normally higher than that of the stator and this difference increases the longer the machine runs [12]. This comparison is, however, only rough as, for example, the absolute temperature of the rotor is unknown to us.

In Figure 6, there is no visible influence of temperature upon magnetizing inductance L_m , which corresponds with theoretical assumptions (see Section 1). Both stator voltage and current were kept almost constant during this warming test (see Figure 7)—stator current was supplied from a converter with a current loop. Because of this, there is a small variance in stator current. We used this variance to show the dependence of L_m on the magnetizing component of the stator current (I_{sd}) in Figure 8, where it is depicted in better scale. This dependence under different loads and frequencies is also shown later in Figure 11. Such a dependence is presented in [11,47], so it can be regarded as another proof of the results obtained by the proposed method.

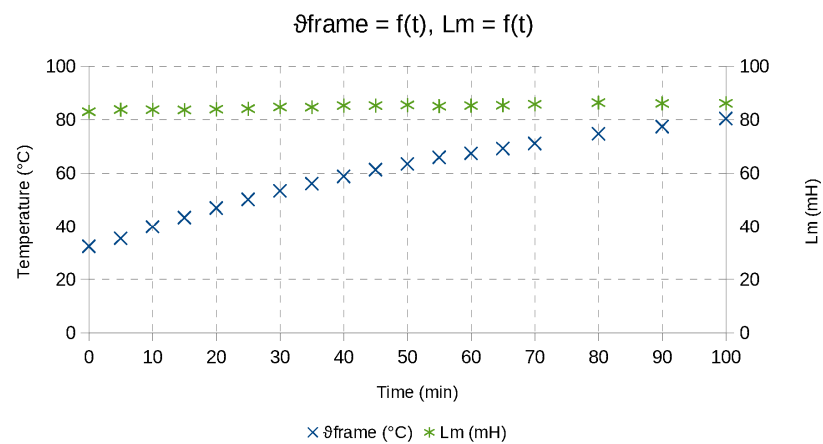


Figure 6. L_m and machine frame temperature ϑ_{frame} in the course of time during warming test.

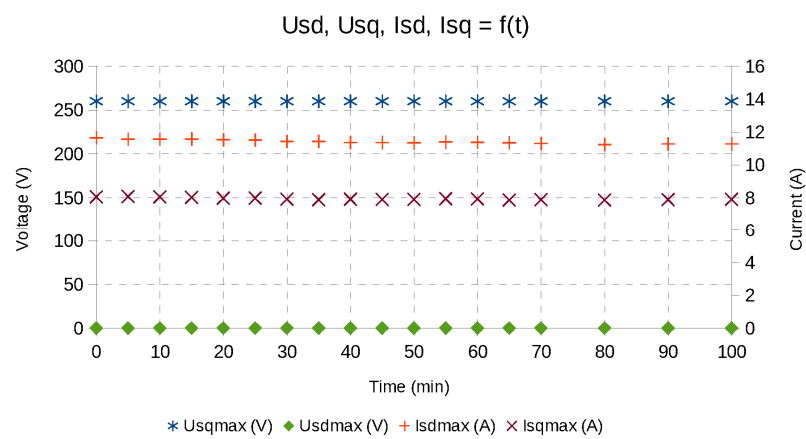


Figure 7. Stator voltage components and stator current components during warming test.

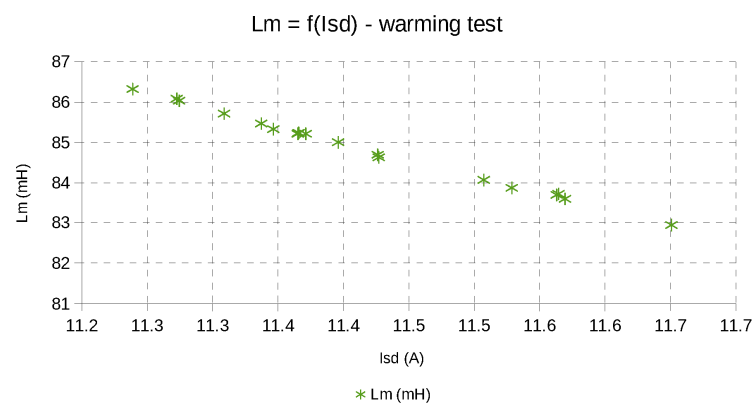


Figure 8. L_m as a function of stator current component I_{sd} during warming test.

4.2. Measurements with Different Loads and Stator Frequencies

Another set of measurements was conducted with different load torques and four different stator frequencies, namely 20, 30, 40, and 50 Hz. Each measurement is represented by five working points with different loads. The temperature difference among measurement points did not exceed 5 °C, so its influence should not be significant in this case. Each measurement point was averaged from five samples with a time span of 10 s.

Stator voltage was set according to the V/f (voltage to frequency) ratio. For measurements at stator frequencies 20, 30, and 40 Hz, this ratio was 6.5. At 50 Hz, the field

weakening area was reached; therefore, the V/f ratio was only 5.6. The voltage vector is again aligned with the q axis, so the d component (V_{sd}) is zero in all presented cases.

The measured data and estimated values of R_r and L_m are presented in the tables below (Tables 3–6). The tables show stator current components I_{sd} and I_{sq} , measured load torque T_{load} , and rotor angular frequency ω_m . The representation of speed by angular frequency was chosen because angular frequency is used in the equations in Section 3. For the calculation of rotations per minute of the shaft, note that the machine has six poles (see Table 1).

Table 3. Measurement at $f_s = 20$ Hz ($\omega_s = 125.66$ rad·s⁻¹) and $V_{sq} = 130$ V.

Measured Input Quantities					
T_{load} (N·m)	9.5	16.0	23.2	30.5	38.5
I_{sd} (A)	9.28	9.01	8.90	9.02	9.37
I_{sq} (A)	3.19	4.66	6.34	8.25	10.41
ω_m (rad·s ⁻¹)	123.58	121.84	119.68	117.14	113.82
f_r (Hz)	0.331	0.609	0.952	1.360	1.890
Estimated Parameters					
R_r (Ω)	0.736	0.826	0.888	0.924	0.972
L_m (mH)	99.2	101.8	103.6	104.3	104.6
Calculated Values of Stator Current Components from T-Equivalent Circuit					
I_{sdc} (A)	9.28	9.01	8.90	9.02	9.37
I_{sqc} (A)	3.19	4.66	6.34	8.25	10.41

Table 4. Measurement at $f_s = 30$ Hz ($\omega_s = 188.50$ rad·s⁻¹) and $V_{sq} = 195$ V.

Measured Input Quantities					
T_{load} (N·m)	9.6	16.0	23.2	30.3	37.8
I_{sd} (A)	9.59	9.46	9.52	9.73	10.10
I_{sq} (A)	2.84	4.22	5.80	7.51	9.31
ω_m (rad·s ⁻¹)	186.41	184.84	182.87	180.75	178.17
f_r (Hz)	0.332	0.581	0.895	1.260	1.640
Estimated Parameters					
R_r (Ω)	0.783	0.847	0.905	0.928	0.967
L_m (mH)	97.5	99.1	99.4	99.3	98.8
Calculated Values of Stator Current Components from T-Equivalent Circuit					
I_{sdc} (A)	9.59	9.46	9.52	9.73	10.10
I_{sqc} (A)	2.84	4.22	5.80	7.51	9.31

Table 5. Measurement at $f_s = 40$ Hz ($\omega_s = 251.33$ rad·s⁻¹) and $V_{sq} = 260$ V.

Measured Input Quantities					
T_{load} (N·m)	9.7	16.0	23.0	30.2	37.9
I_{sd} (A)	9.71	9.67	9.78	10.07	10.48
I_{sq} (A)	2.60	3.92	5.47	7.08	8.76
ω_m (rad·s ⁻¹)	249.24	247.75	245.84	243.91	241.54
f_r (Hz)	0.332	0.570	0.873	1.180	1.550
Estimated Parameters					
R_r (Ω)	0.826	0.878	0.926	0.940	0.976
L_m (mH)	97.0	97.8	97.8	97.0	96.0
Calculated Values of Stator Current Components from T-Equivalent Circuit					
I_{sdc} (A)	9.71	9.67	9.78	10.07	10.48
I_{sqc} (A)	2.60	3.92	5.47	7.08	8.76

Table 6. Measurement at $f_s = 50$ Hz ($\omega_s = 314.16$ rad·s⁻¹) and $V_{sq} = 280$ V.

Measured Input Quantities					
T_{load} (N·m)	9.7	15.6	23.3	30.4	37.4
I_{sd} (A)	7.73	7.88	8.09	8.85	9.44
I_{sq} (A)	2.61	4.13	5.83	7.82	9.52
ω_m (rad·s ⁻¹)	311.36	309.34	306.64	303.85	300.16
f_r (Hz)	0.445	0.776	1.200	1.640	2.230
Estimated Parameters					
R_r (Ω)	0.893	0.931	1.00	0.989	1.07
L_m (mH)	106.5	105.8	106.2	101.3	100.2
Calculated Values of Stator Current Components from T-Equivalent Circuit					
I_{sdc} (A)	7.73	7.88	8.09	8.85	9.44
I_{sqc} (A)	2.61	4.13	5.83	7.82	9.52

It is generally difficult to compare the estimated parameter values with some references. Laboratory standard tests [13], for example, use the line frequency (50 Hz in our case) for locked rotor tests, meaning that slip frequency is equal to 50 Hz. On the other hand, during the operation of the drive with scalar control or IFOC, slip frequency is low (in order of hertz). Magnetizing inductance has a similar problem with the comparison of its estimated value to the value obtained by standard tests: the proposed identification method determines its value for a particular working point, while the standard test value is obtained from no-load measurements. So far, no on-line method has been generally or officially standardized to become a source of reference measurement that other methods could be compared to. As mentioned in the introduction, only R_s is directly measurable in the case of an induction machine with a squirrel cage rotor. Therefore, we compare our results with trends of parameter changes published elsewhere [11,19,28,47] and by a verification scheme described below in this chapter.

To demonstrate that the derivation of the equations of the proposed method is correct, the verification scheme depicted in Figure 9 was proposed.

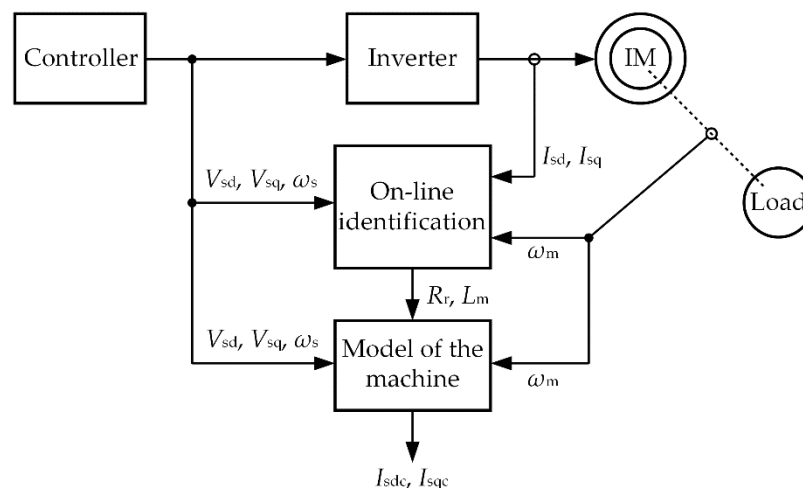


Figure 9. Verification block scheme.

The idea behind this verification scheme is to calculate some measurable quantities from the mathematical model of the machine with the help of estimated parameters and then compare measured and calculated values. In the presented case, stator current components were selected. With the proposed on-line identification method, R_r and L_m were estimated and then their values were used in a mathematical model of the machine. In this model, represented again by a T-equivalent circuit (Figure 2), the knowledge of all

the equivalent circuit parameters and some of the measurable quantities, namely stator voltage components V_{sd} and V_{sq} , stator angular frequency ω_s , and rotor angular frequency ω_m , was used. From these, the stator current components I_{sdc} and I_{sqc} were calculated, with the letter “c” in their subscript standing for “calculated”.

The calculated values of I_{sdc} and I_{sqc} are exactly the same as those that can be measured (I_{sd} , I_{sq}) because this T-equivalent circuit is not capable of introducing some other parasitic effects. Despite this, it demonstrates that the values of R_r and L_m have values appropriate for the T-equivalent circuit representation of the machine.

A number of parameter characteristics can be seen from the presented measurements. Figure 10 shows the dependence of R_r on slip frequency f_r , which corresponds with observations published elsewhere [11,19,28,47]. With the rising load torque T_{load} , the mechanical speed decreased, which resulted in an increase in slip and therefore the slip frequency f_r . There is also a visible influence of stator frequency f_s . R_r is higher mainly due to the skin effect in rotor bars, which is more significant the higher the frequencies are.

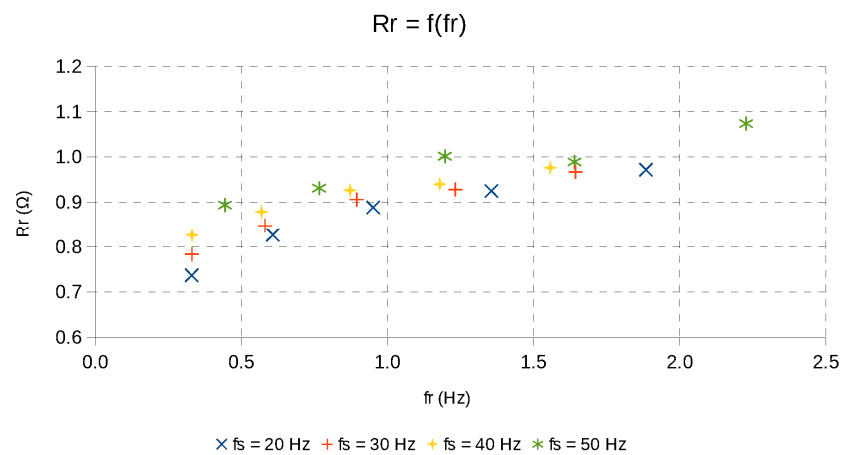


Figure 10. R_r as a function of slip frequency f_r for different stator frequencies f_s .

There is again a visible dependence of L_m on the magnetizing component of stator current component I_{sd} (described in Section 4.1), as shown in Figure 11. In this figure, data from all the measurements with different loads and different frequencies are grouped and the trend corresponds with the results published elsewhere, e.g., in [11,47].

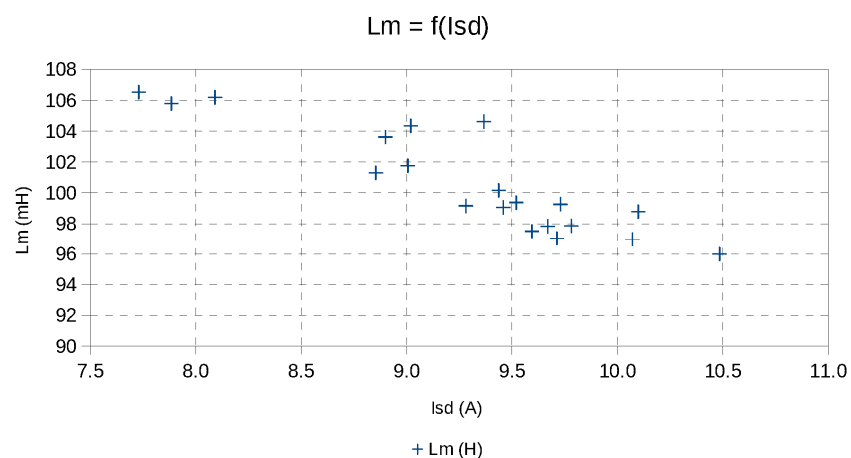


Figure 11. L_m as a function of stator current component I_{sd} from measurements with different loads and different frequencies.

5. Discussion

Due to the character of the results, their interpretation has been carried out in the previous section (Section 4) along with their presentation.

An estimation of the proper value of R_r by the proposed method depends on the accuracy of the speed measurement. If the drive is not equipped with a sensor with a suitable number of pulses per revolution, approaches such as longer measurement or the measurement of the period of the pulse can be deployed. Prolonging the speed measurement should not be a problem as the drive should operate in steady-state mode during measurement. Parameters $L_{\sigma s}$, $L_{\sigma r}$, and R_s are assumed to be constant. This simplification can be performed without a significant loss of accuracy in the case of $L_{\sigma s}$ and $L_{\sigma r}$ as they represent the part of magnetic flux that flows mainly through air. Thus, it is not influenced by a change in temperature and the effect of saturation can also be considered negligible. R_s is, however, influenced by the temperature, but its influence on the calculation is not so significant in most of the operation range. The voltage drop on $L_{\sigma s}$ is higher than that on R_s , and this difference rises with the rising stator frequency and torque-producing stator current component I_{sq} . Moreover, the temperature of the rotor is normally higher than that of the stator [12], which means that the change in R_s is smaller than the change in R_r . Frequency should not have any significant effect on R_s as the stator winding is normally manufactured as parallel filaments to prevent the skin effect.

The proposed method is designated for machines that can be described by a model in the form of a T-equivalent circuit, as presented in Figure 2, which is the majority of induction machines used in industry or traction. An example of a machine type that could not be described with such a model can be a machine with a double rotor cage that would need an additional parallel rotor branch in its equivalent circuit. When the machine conforms to the stated criterion, then the results should be correct regardless of the construction details of the machine. Different construction details would be, however, visible on the results. For example, the change in rotor resistance due to the skin effect caused by slip frequency will depend on the shape of the cross section of the rotor bars. The deeper the bars, the more visible the effective rotor resistance rise due to the skin effect. On the other hand, the wound rotor will not show any significant influence of the skin effect on the rotor resistance as the cross section of the particular winding filaments is small compared to the bars of the squirrel cage.

The shape of the slots (both on the stator and rotor) will have a further effect on the course of magnetizing inductance. Slots whose openings widen towards the air gap (e.g., made for being closed with wedges) will cause the machine to be more sensitive to saturation as this makes the magnetic circuit path narrower compared to closed slots.

The proposed method is thus comparatively universal regardless of the construction features of a particular machine, unless it can be described by a T-equivalent circuit.

Both R_r and L_m can be regarded as slowly varying during steady-state operation. In this mode, R_r is mostly influenced by temperature change, which rises slowly, as can be seen from Figure 5. The flux, which can influence the value of L_m by saturating the magnetic circuit, also does not change quickly during the normal operation of IFOC. Therefore, the method is enough to be executed within minutes during steady-state operation. In the case of a change in a working point of the drive, it should be executed after this change as magnetizing current or slip change can result in a sharp change in R_r or L_m . The averaging of multiple measurements of input quantities is advised to prevent the variation of results.

6. Conclusions

This paper presents a new, computationally modest on-line method for the simultaneous identification of rotor resistance R_r and magnetizing inductance L_m of induction machines. These two parameters are crucial for IFOC, which is a popular control strategy in industrial or traction drives. However, their values change during operation due to the temperature change, frequency, or saturation of the magnetic circuit. Tracking their values can thus improve the performance of the control strategy.

The proposed method utilizes a steady-state voltage model of the machine, which enables a significant simplification of necessary equations. The required quantities are obtained only through equipment that is already present in common electric drives, such as stator current measurement, DC-link voltage measurement, and a speed sensor. It is suitable for drives with resource-constrained microcontrollers that have at least a part of their working cycle in a steady-state mode. The proposed method is designated for machines that can be described by a model in the form of a T-equivalent circuit, which is the majority of induction machines used in industry or traction. When the machine conforms to the stated criterion, then the results should be correct regardless of the construction details of the machine. From the point of view of the overall construction of the drive, a part that can have a significant influence on the results is the speed sensor. This is because the slip of the machine is used for the calculation of R_r . If a sensor with a low number of pulses per revolution is deployed, the measurement of speed can be improved by uncomplicated techniques such as longer measurement or the measurement of the period of the pulse, which will not significantly increase the complexity of the method.

Deriving the method is presented in detail, including a final algorithm of equations for calculation in the microcontroller. Experimental validation was carried out by measurements with different loads at different frequencies and a warming test. Difficulties of the comparison of the resulting values of R_r and L_m to some reference values are presented. To validate the results, two other approaches were therefore used. Firstly, the resulting values of parameters were used in a mathematical model of the machine to calculate stator current components. These calculated stator current components were compared with the measured ones, and both of these values corresponded with each other. This confirms that the resulting values of R_r and L_m are suitable for a working mathematical model of the machine and also confirms that the algorithm of the method is derived correctly. Secondly, the results were further discussed and compared with other publications to prove that the proposed method gives relevant results.

Author Contributions: This article presents the collective work of both authors (T.K. and P.K.). All authors have read and agreed to the published version of the manuscript.

Funding: This research was funded by the Czech CRRC Science and Technology Development Ltd. in Prague, Czech Republic.

Data Availability Statement: The data presented in this study are available on request from the corresponding author. The data are not publicly available due to company restrictions.

Conflicts of Interest: The authors declare no conflict of interest.

Nomenclature

R_s	stator resistance
R_r	rotor resistance
$L_{\sigma s}$	stator leakage inductance
$L_{\sigma r}$	rotor leakage inductance
L_m	magnetizing inductance
V_s, V_{sd}, V_{sq}	stator voltage vector and its components in dq reference frame
I_s, I_{sd}, I_{sq}	stator current vector and its components in dq reference frame
I_{sdc}, I_{sqc}	calculated values of stator current components in dq reference frame
V_i, V_{id}, V_{iq}	back EMF vector and its components in dq reference frame
I_m, I_{md}, I_{mq}	magnetizing current vector and its components in dq reference frame
I_r, I_{rd}, I_{rq}	rotor current vector and its components in dq reference frame

ω_s	stator angular frequency
ω_m	rotor angular frequency
j	imaginary unit
s	slip defined as $s = \frac{\omega_s - \omega_m}{\omega_s}$
R_{req}	equivalent rotor resistance defined as $R_{req} = \frac{R_r}{s}$
P_i	inner machine power
p, q	coefficients of the quadratic equation
$R_{\theta 2}$	value of resistance at elevated temperature
R_{20}	value of resistance at 20 °C
α_{20}	temperature coefficient
$\Delta\theta$	temperature difference
θ_{frame}	machine frame temperature
f_s	stator frequency
f_r	slip frequency
T_{load}	load torque

References

- Wang, F.; Zhang, Z.; Mei, X.; Rodríguez, J.; Kennel, R. Advanced Control Strategies of Induction Machine: Field Oriented Control, Direct Torque Control and Model Predictive Control. *Energies* **2018**, *11*, 120. [\[CrossRef\]](#)
- Tarchała, G.; Orłowska-Kowalska, T. Discrete Sliding Mode Speed Control of Induction Motor Using Time-Varying Switching Line. *Electronics* **2020**, *9*, 185. [\[CrossRef\]](#)
- Alsofyani, I.M.; Lee, K.-B. Evaluation of Direct Torque Control with a Constant-Frequency Torque Regulator under Various Discrete Interleaving Carriers. *Electronics* **2019**, *8*, 820. [\[CrossRef\]](#)
- Hakami, S.S.; Mohd Alsofyani, I.; Lee, K.-B. Low-Speed Performance Improvement of Direct Torque Control for Induction Motor Drives Fed by Three-Level NPC Inverter. *Electronics* **2020**, *9*, 77. [\[CrossRef\]](#)
- Tang, J.; Yang, Y.; Blaabjerg, F.; Chen, J.; Diao, L.; Liu, Z. Parameter Identification of Inverter-Fed Induction Motors: A Review. *Energies* **2018**, *11*, 2194. [\[CrossRef\]](#)
- Zhao, L.; Huang, J.; Chen, J.; Ye, M. A Parallel Speed and Rotor Time Constant Identification Scheme for Indirect Field Oriented Induction Motor Drives. *IEEE Trans. Power Electron.* **2016**, *31*, 6494–6503. [\[CrossRef\]](#)
- Karlovsky, P.; Lipcak, O.; Bauer, J. Iron Loss Minimization Strategy for Predictive Torque Control of Induction Motor. *Electronics* **2020**, *9*, 566. [\[CrossRef\]](#)
- Alkorta, P.; Barambones, O.; Cortajarena, J.A.; Martija, I.; Maseda, F.J. Effective Position Control for a Three-Phase Motor. *Electronics* **2020**, *9*, 241. [\[CrossRef\]](#)
- Ortega-García, L.E.; Rodríguez-Sotelo, D.; Nuñez-Perez, J.C.; Sandoval-Ibarra, Y.; Perez-Pinal, F.J. DSP-HIL Comparison between IM Drive Control Strategies. *Electronics* **2021**, *10*, 921. [\[CrossRef\]](#)
- Lin, F.J.; Su, M.S. A High-Performance Induction Motor Drive with on-Line Rotor Time-Constant Estimation. *IEEE Trans. Energy Convers.* **1997**, *12*, 297–303. [\[CrossRef\]](#)
- Keyhani, A.; Lu, W.; Proca, B. Modeling and Parameter Identification of Electric Machines. In *Handbook of Automotive Power Electronics and Motor Drives*; CRC Press: Boca Raton, FL, USA; Taylor & Francis Group: Abingdon, UK, 2017; pp. 449–514, ISBN 978-1-315-22090-1.
- Tran, T.-V.; Nègre, E. Efficient Estimator of Rotor Temperature Designing for Electric and Hybrid Powertrain Platform. *Electronics* **2020**, *9*, 1096. [\[CrossRef\]](#)
- IEEE Standard Test Procedure for Polyphase Induction Motors and Generators*; IEEE Std 112-2017 (Revision of IEEE Std 112-2004); IEEE: Piscataway, NJ, USA, 2018; pp. 1–115. [\[CrossRef\]](#)
- Mölsä, E.; Tiitinen, L.; Saarakkala, S.; Peretti, L.; Hinkkanen, M. Standstill Self-Commissioning of an Induction Motor Drive. In Proceedings of the 2020 IEEE Energy Conversion Congress and Exposition (ECCE), Detroit, MI, USA, 11–15 October 2020; pp. 3044–3050.
- Peresada, S.; Kovbasa, S.; Prystupa, D.; Lyshevski, S.E. Identification of Induction Motor Parameters for Self-Commissioning Procedure: A New Algorithm and Experimental Verification. In Proceedings of the 2014 IEEE 23rd International Symposium on Industrial Electronics (ISIE), Istanbul, Turkey, 1–4 June 2014; pp. 818–823.
- Khojakhani, Y.; Choo, K.-M.; Won, C.-Y. Stator Inductance Identification Based on Low-Speed Tests for Three-Level NPC Inverter-Fed Induction Motor Drives. *Electronics* **2020**, *9*, 183. [\[CrossRef\]](#)
- Khamehchi, S.; Mölsä, E.; Hinkkanen, M. Comparison of Standstill Parameter Identification Methods for Induction Motors. In Proceedings of the 2018 IEEE 9th International Symposium on Sensorless Control for Electrical Drives (SLED), Helsinki, Finland, 13–14 September 2018; pp. 156–161.
- Toliyat, H.A.; Levi, E.; Raina, M. A Review of RFO Induction Motor Parameter Estimation Techniques. *IEEE Trans. Energy Convers.* **2003**, *18*, 271–283. [\[CrossRef\]](#)

19. Tang, J.; Yang, Y.; Diao, L.; Chen, J.; Chang, Y.; Liu, Z. Parameter Identification of Induction Motors for Railway Traction Applications. In Proceedings of the 2018 IEEE Energy Conversion Congress and Exposition (ECCE), Portland, ON, USA, 23–27 September 2018; pp. 284–288.
20. Tuovinen, T.; Hinkkanen, M.; Luomi, J. Modeling of Saturation Due to Main and Leakage Flux Interaction in Induction Machines. *IEEE Trans. Ind. Appl.* **2010**, *46*, 937–945. [[CrossRef](#)]
21. Lipcak, O.; Bauer, J.; Chomat, M. Reactive Power MRAS for Rotor Resistance Estimation Taking Into Account Load-Dependent Saturation of Induction Motor. In Proceedings of the 2019 International Conference on Electrical Drives Power Electronics (EDPE), Košice, Slovakia, 22–24 September 2019; pp. 255–260.
22. Zhang, J.; Chai, J.; Sun, X.; Lu, H. On-Line Parameter Estimation for Indirect Field Oriented Control of Induction Machine Based on Steady State Voltage Model. In Proceedings of the IECON 2014—40th Annual Conference of the IEEE Industrial Electronics Society, Dallas, TX, USA, 29 October–1 November 2014; pp. 769–773.
23. Quintero-Manriquez, E.; Sanchez, E.N.; Harley, R.G.; Li, S.; Felix, R.A. Neural Inverse Optimal Control Implementation for Induction Motors via Rapid Control Prototyping. *IEEE Trans. Power Electron.* **2019**, *34*, 5981–5992. [[CrossRef](#)]
24. Liu, Y. Multi-Parameter Online Identification Algorithm of Induction Motor for Hybrid Electric Vehicle Applications. In Proceedings of the 2014 Sixth International Symposium on Parallel Architectures, Algorithms and Programming, Beijing, China, 13–15 July 2014; pp. 35–39.
25. Kandoussi, Z.; Boulghasoul, Z.; Elbacha, A.; Tajer, A. Luenberger Observer Based Sensorless Indirect FOC with Stator Resistance Adaptation. In Proceedings of the 2014 Second World Conference on Complex Systems (WCCS), Agadir, Morocco, 10–12 November 2014; pp. 367–373.
26. Stinga, F.; Soimu, A.; Marian, M. Online Estimation and Control of an Induction Motor. In Proceedings of the 2015 19th International Conference on System Theory, Control and Computing (ICSTCC), Cheile Gradistei, Romania, 14–16 October 2015; pp. 742–746.
27. Zaky, M.S.; Khater, M.M.; Shokralla, S.S.; Yasin, H.A. Wide-Speed-Range Estimation With Online Parameter Identification Schemes of Sensorless Induction Motor Drives. *IEEE Trans. Ind. Electron.* **2009**, *56*, 1699–1707. [[CrossRef](#)]
28. Chen, J.; Huang, J.; Sun, Y. Resistances and Speed Estimation in Sensorless Induction Motor Drives Using a Model With Known Regressors. *IEEE Trans. Ind. Electron.* **2019**, *66*, 2659–2667. [[CrossRef](#)]
29. Radhakrishnan, K.; Unnikrishnan, A.; Balakrishnan, K. EM Based Extended Kalman Filter for Estimation of Rotor Time-Constant of Induction Motor. In Proceedings of the IEEE International Symposium on Industrial Electronics, 2006 IEEE International Symposium on Industrial Electronics, Montreal, QC, Canada, 9–13 July 2006; pp. 2434–2438.
30. Buchholz, O.; Böcker, J.; Bonifacio, J. Online-Identification of the Induction Machine Parameters Using the Extended Kalman Filter. In Proceedings of the 2018 XIII International Conference on Electrical Machines (ICEM), Alexandroupoli, Greece, 3–6 September 2018; pp. 1623–1629.
31. Li, J.; Nie, S.; Meng, Q.; Ren, H. Efficiency Optimization of Induction Motors Based on Online Identification of Iron Loss Equivalent Resistance via Dual Extended Kalman Filter. In Proceedings of the 2016 IEEE Region 10 Conference (TENCON), Singapore, 22–25 November 2016; pp. 3309–3312.
32. Kamankesh, S.; Khaburi, D.A. On-Line Rotor Time Constant Estimation for Induction Motor Using Two New Methods, RLS and SDBP Algorithms. In Proceedings of the 2009 International Conference on Electrical and Electronics Engineering—ELECO 2009, Bursa, Turkey, 5–8 November 2009; pp. 1–184.
33. Telford, D.; Dunnigan, M.W.; Williams, B.W. Online Identification of Induction Machine Electrical Parameters for Vector Control Loop Tuning. *IEEE Trans. Ind. Electron.* **2003**, *50*, 253–261. [[CrossRef](#)]
34. Cirrincione, M.; Pucci, M.; Cirrincione, G.; Capolino, G.-A. A New Experimental Application of Least-Squares Techniques for the Estimation of the Induction Motor Parameters. *IEEE Trans. Ind. Appl.* **2003**, *39*, 1247–1256. [[CrossRef](#)]
35. Huynh, D.C.; Dunnigan, M.W.; Finney, S.J. On-Line Parameter Estimation of an Induction Machine Using a Recursive Least-Squares Algorithm with Multiple Time-Varying Forgetting Factors. In Proceedings of the 2010 IEEE International Conference on Power and Energy, Kuala Lumpur, Malaysia, 29 November–1 December 2010; pp. 444–449.
36. Maiti, S.; Chakraborty, C.; Hori, Y.; Ta, M.C. Model Reference Adaptive Controller-Based Rotor Resistance and Speed Estimation Techniques for Vector Controlled Induction Motor Drive Utilizing Reactive Power. *IEEE Trans. Ind. Electron.* **2008**, *55*, 594–601. [[CrossRef](#)]
37. Basic, M.; Vukadinovic, D.; Grgic, I.; Bubalo, M. Speed-Sensorless Vector Control of an Induction Generator Including Stray Load and Iron Losses and Online Parameter Tuning. *IEEE Trans. Energy Convers.* **2020**, *35*, 724–732. [[CrossRef](#)]
38. He, L.; Restrepo, J.; Cheng, S.; Harley, R.G.; Habetler, T.G. An Improved DC-Signal-Injection Method with Active Torque-Ripple Mitigation for Thermal Monitoring of Field-Oriented-Controlled Induction Motors. In Proceedings of the 2015 IEEE Energy Conversion Congress and Exposition (ECCE), Montreal, QC, Canada, 20–24 September 2015; pp. 4447–4454.
39. Baneira, F.; Yepes, A.G.; López, Ó.; Doval-Gandoy, J. Estimation Method of Stator Winding Temperature for Dual Three-Phase Machines Based on DC-Signal Injection. *IEEE Trans. Power Electron.* **2016**, *31*, 5141–5148. [[CrossRef](#)]
40. Samoseiko, V.F.; Saushev, A.V.; Belousova, N.V. Asynchronous Motor Control Algorithm with Parameter Identification. In Proceedings of the 2019 International Ural Conference on Electrical Power Engineering (UralCon), Chelyabinsk, Russia, 1–3 October 2019; pp. 284–289.

41. Wang, L.; Deng, X.; Hu, K.; Zhang, X.; Wang, K. A Novel Parameter Identification Method for Induction Motor. In Proceedings of the 2010 International Conference on Measuring Technology and Mechatronics Automation, Changsha, China, 13–14 March 2010; pp. 265–268.
42. Vázquez-Gutiérrez, Y.; O’Sullivan, D.L.; Kavanagh, R.C. Small-Signal Modeling of the Incremental Optical Encoder for Motor Control. *IEEE Trans. Ind. Electron.* **2020**, *67*, 3452–3461. [[CrossRef](#)]
43. Brugnano, F.; Concari, C.; Imamovic, E.; Savi, F.; Toscani, A.; Zanichelli, R. A Simple and Accurate Algorithm for Speed Measurement in Electric Drives Using Incremental Encoder. In Proceedings of the IECON 2017—43rd Annual Conference of the IEEE Industrial Electronics Society, Beijing China, 29 October–1 November 2017; pp. 8551–8556.
44. Anuchin, A.; Astakhova, V.; Shpak, D.; Zharkov, A.; Briz, F. Optimized Method for Speed Estimation Using Incremental Encoder. In Proceedings of the 2017 International Symposium on Power Electronics (Ee), Novi Sad, Serbia, 19 October 2017; pp. 1–5.
45. Pichlík, P.; Bauer, J. Analysis of the Locomotive Wheel Slip Controller Operation During Low Velocity. *IEEE Trans. Intell. Transp. Syst.* **2020**, *22*, 1543–1552. [[CrossRef](#)]
46. Han, J.; Xu, J.; Zhu, G.; Song, J.; Wang, Y. A Novel Voltage Reconstruction Method for MRAS-Based Sensorless Induction Motor Drives at Low Switching Frequency. In Proceedings of the 2020 IEEE 9th International Power Electronics and Motion Control Conference (IPEMC2020-ECCE Asia), Nanjing, China, 29 November 2020; pp. 336–341.
47. Sudhoff, S.D.; Aliprantis, D.C.; Kuhn, B.T.; Chapman, P.L. Experimental Characterization Procedure for Use with an Advanced Induction Machine Model. *IEEE Trans. Energy Convers.* **2003**, *18*, 48–56. [[CrossRef](#)]